EFFECT OF STRAIN PATH ON MICROSTRUCTURE AND MECHANICAL PROPERTIES IN COLD - ROLLED $[FeNi]_{69}Cr_{15}Mn_{10}Nb_6$ HIGH - ENTROPY ALLOY

Majid Naseri[1], Abdrakhman Naizabekov[2], Dmitry Mikhailov[1], Sergey Legnev[1], Nataliya Shaburova[1], Anatoliy Pellenen[1], Evgenii Bodrov[1], Marina Samodurova[1], Evgeny Trofimov[1], Evgeniy Panin[1]

[1]*South Ural State University, 76 Lenin Av. Chelyabinsk 454080, Russia.*
[2]*Rudny Industrial University, 38 50 let Oktyabrya St. Rudny, 111500 Kazakhstan*
E-mail: naserim@susu.ru, sergey_legnev@mail.ru

Received 03 April 2024
Accepted 05 July 2024
DOI: 10.59957/jctm.v59.i5.2024.27

ABSTRACT

$[FeNi]_{69}Cr_{15}Mn_{10}Nb_6$ high - entropy alloys (HEAs) were subjected to heavy cold-rolling process at ambient temperature through two distinct routes, namely unidirectional cold-rolling (UCR) and multistep cross cold-rolling (MSCCR) routes, to investigate the effect of the strain path on the microstructure and mechanical properties of the alloys. In the MSCCR route, the specimen rotated 90° around the normal direction axis between each cycle. The as-homogenized specimen revealed a two-phase microstructure consisting of FeNiNb - rich dendrites distributed in a nearly homogenous face-centered cubic (FCC) HEA matrix. Here, FeNiNb - rich dendrites were elongated, broken down, and stretched along the rolling direction during both processing routes. In the MSCCR - processed specimen, the dendrites exhibited a smaller average size with a more uniform distribution compared to that of the UCR specimen, which could be mainly ascribed to the elongation mechanisms in the normal and transverse directions during the MSCCR route. These microstructural features, introduced through MSCCR, appeared to be most prone to shear band formation and grain refinement. The MSCCR - processed specimen shows a microhardness of 445 HV, a tensile strength of 1245 MPa, and a remarkable elongation of 16 % at ambient temperature, outperforming the UCR-processed specimen with a microhardness of 418 HV, a tensile strength of 1180 MPa, and an elongation of 14 %. The superior mechanical properties of the MSCCR - processed specimen are attributed to its refined microstructure, increased dislocation density, and uniform distribution of FeNiNb - rich dendrites within the microstructure.

Keywords: high entropy alloys, heavy cold-rolling, strain path, microstructure evolution, mechanical characterization.

INTRODUCTION

Multicomponent metallic alloys known as high-entropy alloys (HEAs) have been developed using the breakthrough alloy design strategy of mixing the alloying elements at equiatomic or nearly equiatomic concentrations and have captured the interest of materials scientists [1, 2]. Generally, HEAs have several substantially higher properties than conventional alloys, including excellent wear resistance, outstanding corrosion resistance, high strength and hardness at elevated temperatures, and exceptional thermal stability. Hence, the last few years have seen significant efforts to enhance the mechanical properties of HEAs for commercial applications [3 - 8].

The mechanical properties of HEAs are determined by their microstructure, and their characteristics can be further enhanced in comparison to as-cast materials by developing appropriate processing routes. Over the past decade, researchers have investigated the microstructure and mechanical properties of numerous HEAs as a result of changes in processing factors, including the starting grain size [9, 10], cryorolling [11 - 13], heating rate [11, 14], and imposed strain [15 - 17]. It should be noted that the strain path is another important processing parameter that has a significant effect on the microstructure of materials. Traditional single-directional rolling and cross-rolling are the two main types of strain paths in rolling processes. The specimen is rotated around the normal direction (ND) during a typical cross-rolling pass, thereby mutually exchanging the transverse direction (TD) and rolling direction (RD). The effect of the cross-rolling process on the microstructure and properties of different metals and metal matrix composites (MMCs) has been extensively investigated. Previous works demonstrated that strain path has a major effect on the microstructure and mechanical characteristics of alloys [18 - 23].

Nowadays, it is well known that the focus of HEAs research is to tailor the composition to develop new materials with superior properties to pave the way for their practical applications. Moreover, further possibilities for enhancing the mechanical properties of HEAs are also provided by post-processes, i.e., heat treatment and plastic deformation. For the HEAs, cold rolling is a simple and efficient post-fabrication technique that induces a textured microstructure for the desired characteristics. In this regard, strain path is a fascinating rolling parameter that can severely influence the microstructure and subsequent mechanical characteristics of HEAs [24, 25].

This study is the first of its kind to focus on the effect of strain path on the evolution of microstructure and mechanical properties in cold-rolled $[FeNi]_{69}Cr_{15}Mn_{10}Nb_6$ HEA. Due to the importance of HEAs in providing desirable engineering properties, it is believed that clarifying the effect of cross-rolling in HEAs would attract great interest among scientists.

EXPERIMENTAL

The $[FeNi]_{69}Cr_{15}Mn_{10}Nb_6$ (in at. %) ingot was initially prepared through vacuum melting the constituent elements with 99.9 wt.% purity at temperatures of 1673 - 1723°C. Subsequently, the alloy ingot was homogenized at 1173 K for 10 hours in a furnace and then air-quenched. The as-homogenized specimens were deformed up to 90 % reduction in thickness (corresponding to a total equivalent strain of 2.65) using two cold-rolling routes (Fig. 1) unidirectional cold-rolling (UCR) and multistep cross cold-rolling (MSCCR). During MSCCR, a change in the strain path was implemented by rotating the specimens 90° around the ND at the end of each cycle. A laboratory rolling machine with a 20 tons loading capacity was used to accomplish the cold rolling process with no lubrication. In this experiment, the roll peripheral speed was approximately 3 m min^{-1}, and the roll diameter was 180 mm.

Microstructural evolution during cold rolling was studied using a field emission scanning electron microscope (FE-SEM, JEOL JSM7001F, Japan) equipped with an energy dispersive X - ray spectroscopy detector (EDS, Oxford INCA X-max 80, Oxford Instruments, Great Britain) for chemical composition

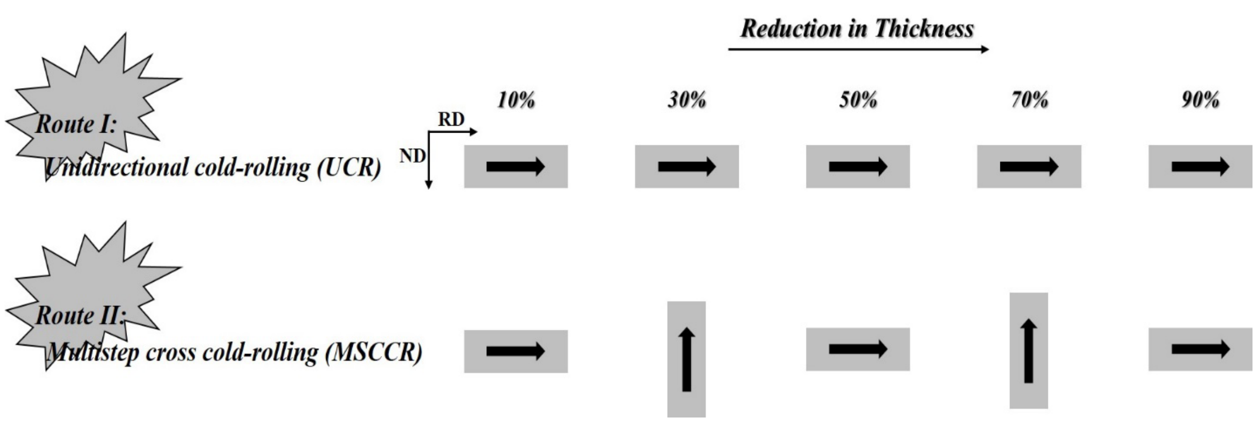

Fig. 1. Schematic illustration showing the UCR and MSCCR processing routes.

analysis. Transmission electron microscopy (TEM, JEM 1200 JEOL, Japan) was utilized to provide information about dislocations and substructure features. The phase structure of the specimens was explored by X - ray diffraction (XRD) using Cu Kα radiation and a scanning speed of 2° min^{-1} over a 2θ range of 5° to 95°. Rigaku Ultima IV X-ray diffractometer (Rigaku, Japan) was employed, and the measurements were carried out at 40 kV with a tube current of 20 mA.

The Vickers microhardness (HV) of the specimens was determined on the rolling direction-transverse direction (RD - TD) plane under a load of 100 g for 15 s. Electro-discharge machining was used to cut miniature tensile specimens with gauge dimensions of 1.1 mm × 1.0 mm × 0.6 mm according to the rolling (RD), transverse (TD), and normal (ND) directions, respectively. Tensile tests were conducted on a Hounsfield H50KS tensile testing machine (Tinius Olsen Ltd., Redhill, UK) at a nominal strain rate of 10^{-3} s^{-1}.

RESULTS AND DISCUSSION

Fig. 2 shows the back scattered electron SEM (BSE4 - SEM) image and the corresponding EDS maps of the as - homogenized $[FeNi]_{69}Cr_{15}Mn_{10}Nb_6$ HEA. Severe elemental segregation can be seen in various parts of the microstructure of the specimen. The results of the EDS chemical analysis are shown in Table 1. The microstructure of $[FeNi]_{69}Cr_{15}Mn_{10}Nb_6$ HEA is composed of FeNiNb - rich bright - gray dendrites distributed within a nearly homogenous HEA matrix, which is seen as a dark-gray matrix in the BSE - SEM image (Fig. 2). The EDS maps indicate a homogenous distribution of Fe, Ni, Cr, and Mn in the dark-gray matrix region. The bright-gray dendrites are mainly rich in Nb and to a lower extent in Fe and Ni (Table 1).

Fig. 3 shows the BSE-SEM images and the corresponding EDS maps of the UCR and MSCCR-processed $[FeNi]_{69}Cr_{15}Mn_{10}Nb_6$ HEA. After 90 %

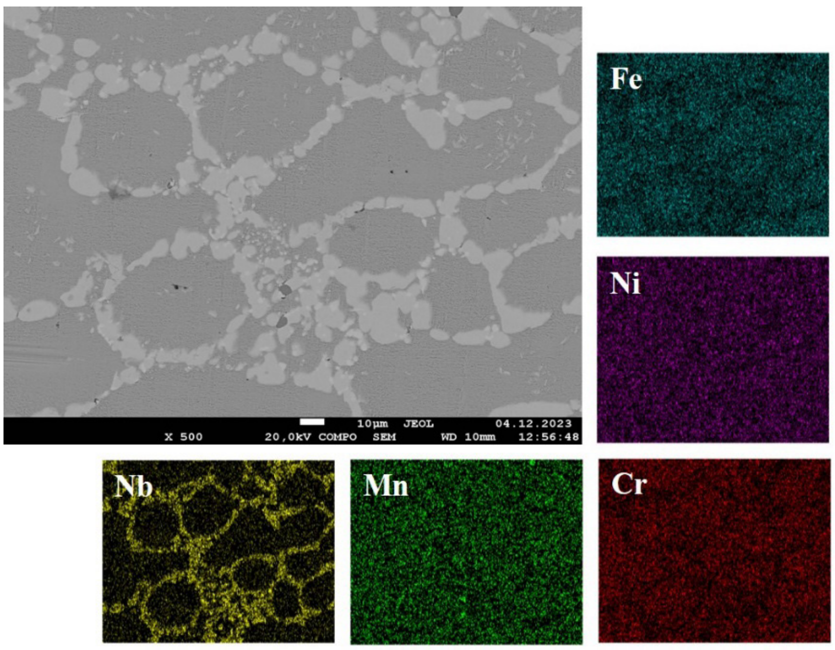

Fig. 2. BSE-SEM images and the corresponding EDS maps for the as - homogenized $[FeNi]_{69}Cr_{15}Mn_{10}Nb_6$ specimen.

Table 1. Chemical composition of the dendrite and matrix regions in the as - homogenized $[FeNi]_{69}Cr_{15}Mn_{10}Nb_6$ specimen.

Composition, EDS, at. %						
		Fe	Ni	Cr	Mn	Nb
$[FeNi]_{69}Cr_{15}Mn_{10}Nb_6$	Dendrite	19.90	18.99	5.96	4.85	50.30
	Matrix	40.64	32.81	17.41	6.68	2.46

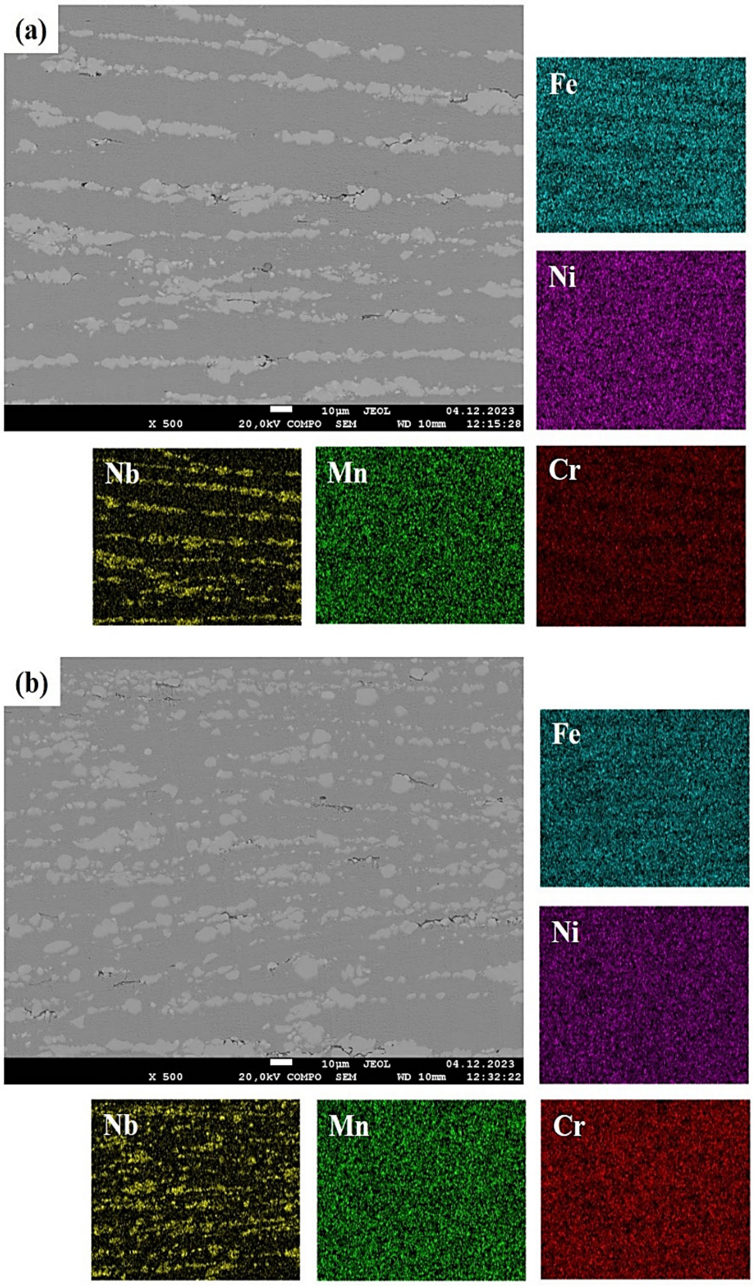

Fig. 3. BSE-SEM images and the corresponding EDS maps for the (a) UCR and (b) MSCCR-processed $[FeNi]_{69}Cr_{15}Mn_{10}Nb_6$ HEA deformed up to a 90 % reduction in thickness.

reduction in thickness (Fig. 3a, b), the FeNiNb dendrites are broken and stretched along the rolling direction in both cold-rolling routes. Also, the arm spacing between primary dendrites is reduced. As a result, this indicates refinement of the as-cast coarse dendritic microstructure under heavy cold-rolling. In addition, BSE-SEM images indicate the presence of coarse and fine dendrites in the microstructures of both specimens. It is obvious that the composition of coarse and fine dendrites is identical since long-range diffusion is prohibited at ambient temperature in the alloy. However, Fig. 3b shows that the amount of fine FeNiNb - rich dendrites in the MSCCR-processed specimen is higher than that of the UCR - processed specimen. Moreover, MSCCR results in a more uniform distribution of the dendrites within the microstructure of HEA. During MSCCR,

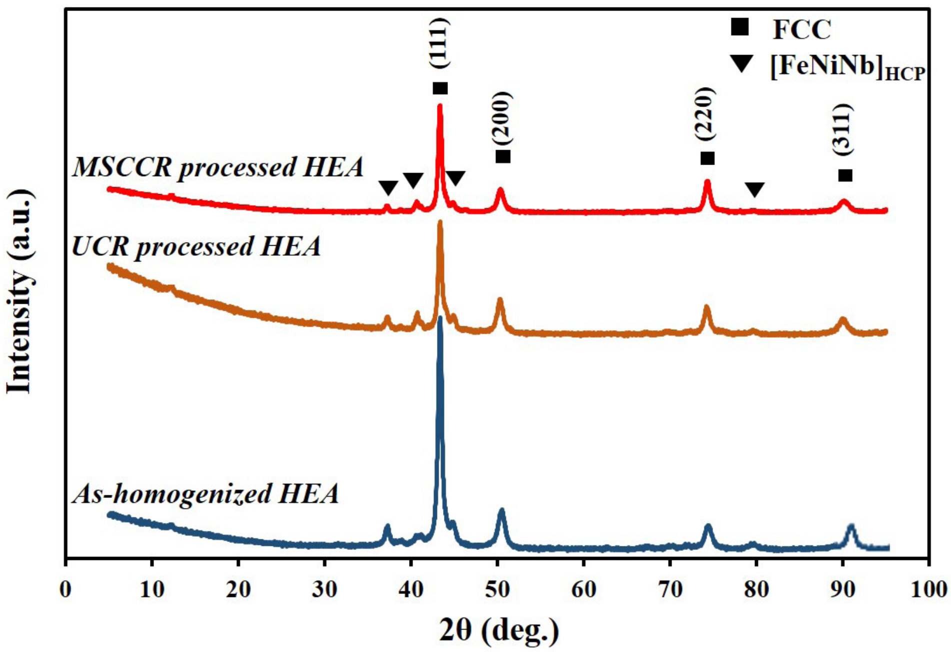

Fig. 4. XRD patterns for the as-homogenized, UCR, and MSCCR - processed $[FeNi]_{69}Cr_{15}Mn_{10}Nb_6$ HEAs deformed up to a 90 % reduction in thickness.

FeNiNb - rich dendrites are alternately stretched parallel to and perpendicular to the RD in successive cycles due to the specimen rotation around the ND. As a result, dendritic arms undergo elongation in both longitudinal and transverse directions; hence, they can be more severely broken and redistributed within the microstructure. Hence, the result is a finer and more homogenous microstructure in the MSCCR - processed specimen than in the UCR - processed one.

XRD patterns of the HEAs in their as - homogenized and cold-rolled states are shown in Fig. 4. The XRD patterns indicate the presence of FCC solid solution as the main phase and a minor amount of FeNiNb - based secondary phase. No significant intermetallic or oxide phases are observed in the as - homogenized and cold-rolled specimens. The full width at half maximum (FWHM) of the Bragg diffraction peaks indicates that the peak intensities of all lattice planes gradually decrease during cold rolling. The trend suggests that heavy cold-rolling induces the accumulation of structural defects, grain and/or crystallite size refinement, and distortion in crystal orientation [19, 26 - 28]. In other words, the heavy cold-rolling process resulted in peak broadening.

Fig. 5 demonstrates the TEM microstructure of the UCR and MSCCR - processed $[FeNi]_{69}Cr_{15}Mn_{10}Nb_6$ HEA, which deformed up to 90 % reduction in thickness in the RD - TD plane. As can be seen, a high density of dislocations is present within the grain and at the grain boundaries, making the grain boundaries unclear and hard to visualize in the TEM images. The matrix grain size in MSCCR-processed HEA is smaller than that of the UCR specimen. In cold rolling structures, there are essentially two kinds of boundaries: lamellar boundaries (LBs), which are nearly parallel to the rolling plane, and short transverse boundaries that connect LBs. During the MSCCR, the specimen rotation around ND causes LBs to alternately become parallel and perpendicular to RD in subsequent cycles during the MSCCR, as explained in the experimental section. Therefore, the interconnecting boundary spacing in the MSCCR specimen is less than that of the UCR specimen. Consequently, MSCCR leads to more effective grain refinement when compared to the UCR since it greatly reduces the aspect ratio of the interconnecting boundary spacing and the lamellar boundary spacing. This result is consistent with the previously reported results on the nanostructured materials processed by cross accumulative roll bonding (CARB) [19 - 21, 29, 30].

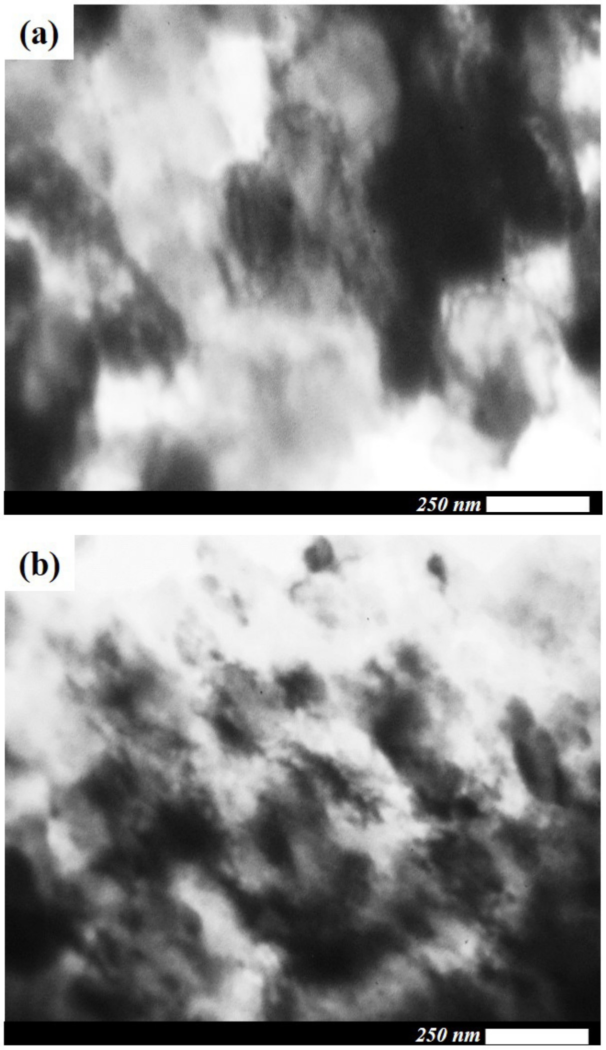

Fig. 5. TEM micrographs from the RD-TD plane for the (a) UCR and (b) MSCCR-processed $[FeNi]_{69}Cr_{15}Mn_{10}Nb_6$ HEA deformed up to a 90 % reduction in thickness.

In order to quantitatively investigate dislocation density during the heavy cold-rolling process, a method based on the indentation size effect (ISE) can be used [31]. According to this theory, the dislocation density (ρ) can be estimated from the microhardness value using Eq. 1 [31].

$$\rho = \frac{HV^2}{27\alpha^2 G^2 b^2} - \frac{3\sqrt{2}}{\sqrt{1.72\pi}} \frac{\sqrt{HV}\cot\varphi}{\pi b\sqrt{F}} \quad (1)$$

where HV is the Vickers microhardness, φ is equal to 68°, α is considered 0.3 in this work, G is elastic shear modulus (~81 GPa for the $[FeNi]_{69}Cr_{15}Mn_{10}Nb_6$ HEA [32]), b is the Burgers vector (0.255 nm [32]), and F is the applied force to the indenter. Table 2 shows the microhardness and dislocation density for the as-homogenized, UCR, and MSCCR processed $[FeNi]_{69}Cr_{15}Mn_{10}Nb_6$ HEA with a 90 % reduction in thickness. After a 90 % reduction in thickness, a significant increase in microhardness is observed. The microhardness of $[FeNi]_{69}Cr_{15}Mn_{10}Nb_6$ HEA increased from 276 HV to 418 HV for the UCR-processed specimen and to 445 HV for the MSCCR specimen, which is almost 1.52 and 1.62 times greater than that of the as-homogenized specimen. This significant increase in microhardness after 90 % reduction in thickness can be explained by strain hardening and increase in dislocation density [33 - 36], which are followed by the interaction and rearrangement of dislocations and the formation of dislocation cell walls and sub-grain boundaries (Fig. 5).

Engineering stress-strain curves of the as-homogenized, UCR, and MSCCR - processed $[FeNi]_{69}Cr_{15}Mn_{10}Nb_6$ HEA deformed up to 90 % reduction in thickness are shown in Fig. 6. After heavy cold-rolling, it is obvious that tensile strength improved for both UCR and MSCCR - processed $[FeNi]_{69}Cr_{15}Mn_{10}Nb_6$ HEA. As can be observed, the specimen subjected to MSCCR exhibits better tensile

Table 2. Microhardness and dislocation density of as-homogenized, UCR, and MSCCR - processed $[FeNi]_{69}Cr_{15}Mn_{10}Nb_6$ HEA deformed up to a 90 % reduction in thickness.

	Vickers microhardness, HV	Dislocation density, x10^5 nm^{-2}
As - homogenized HEA	276	3.24
UCR processed HEA	418	9.63
MSCCR processed HEA	445	10.85

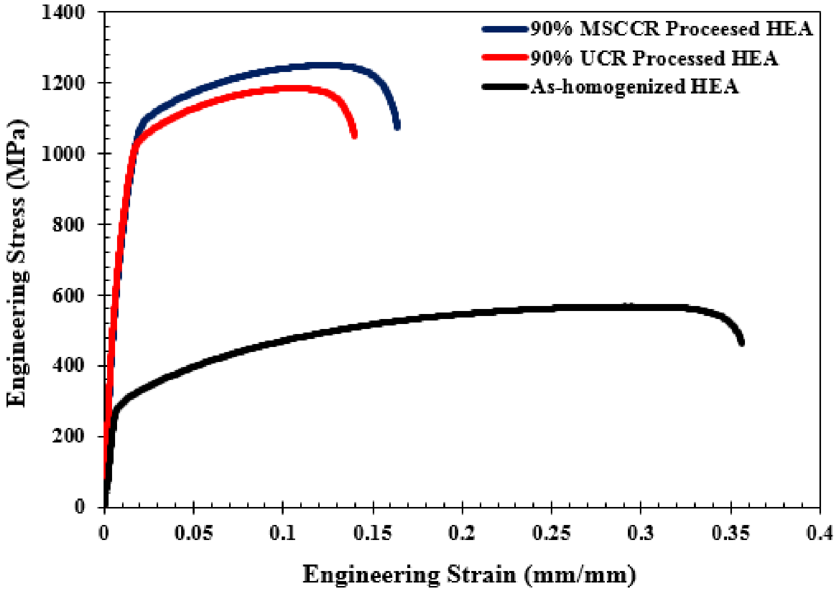

Fig. 6. Stress-strain curves for the as - homogenized, UCR, and MSCCR - processed $[FeNi]_{69}Cr_{15}Mn_{10}Nb_6$ HEAs deformed up to a 90 % reduction in thickness.

characteristics compared to the UCR - processed specimen. The tensile strength of the UCR and MSCCR-processed $[FeNi]_{69}Cr_{15}Mn_{10}Nb_6$ HEA reaches about 1180 MPa and 1245 MPa, respectively. This superior tensile behaviour realized after MSCCR can be mainly ascribed to the change in strain path during MSCCR, which allows for a higher dislocation density to be achieved. As expressed by Cabibbo et al. , it is possible to activate new slip systems and increase dislocation density at the grain boundaries during strain path change in the equal-channel angular pressing/extrusion (ECAP/ECAE) process [37]. It is concluded that, compared to UCR with a constant strain path, the rate of formation of submicron grains during MSCCR is higher.

A comparison of elongation between UCR and MSCCR - processed $[FeNi]_{69}Cr_{15}Mn_{10}Nb_6$ HEA indicates that the elongation of the MSCCR specimen is higher than that of the UCR specimen. Similar observations have been previously reported by researchers [25, 27]. Two reasons can be responsible for this phenomenon. The first is that elongation occurs in normal and transverse directions during MSCCR, resulting in a more homogeneous distribution of finer FeNiNb - rich dendrites in the microstructure (Fig. 3). The second is that the average grain size and their aspect ratio become smaller during MSCCR (Fig. 5). On the other hand, numerous boundaries act as barriers and impede the growth of cracks, causing a higher ductility in MSCCR.

CONCLUSIONS

The effect of strain path on the microstructural characterization and mechanical properties of $[FeNi]_{69}Cr_{15}Mn_{10}Nb_6$ (HEAs) processed by unidirectional cold-rolling (UCR) and multistep cross cold-rolling (MSCCR) was investigated. A change in strain path was imposed MSCCR by rotating the specimen 90° around the normal direction after each cycle. The microstructure of the as-homogenized $[FeNi]_{69}Cr_{15}Mn_{10}Nb_6$ HEAs revealed that FeNiNb-rich dendrites are distributed in a nearly homogenous FCC HEA matrix. In both UCR and MSCCR processes, FeNiNb-rich dendrites are broken down and stretched along the rolling direction. The average size of broken dendrites and their distribution in the MSCCR specimen is finer and more uniform compared to the UCR specimen due to the specimen elongation mechanisms in normal and transverse directions during MSCCR. While both routes resulted in a significant improvement in the mechanical properties of the specimens at room temperature, the MSCCR-processed specimen exhibited superior mechanical properties (higher microhardness, strength, and ductility). This is due to the smaller grain sizes, increased dislocation density, and more homogenous distribution of finer dendrites in the HEA matrix achieved during the MSCCR.

Acknowledgments

The work was supported financially by the Russian Federation represented by Ministry of Science and Higher Education of the Russian Federation, project number No. 075-15-2023-614.

REFERENCES

1. B. Cantor, I.T.H. Chang, P. Knight, A.J.B. Vincent, Microstructural development in equiatomic multicomponent alloys, Materials Science and Engineering: A, 375-377, 2004, 213-218. https://doi.org/10.1016/j.msea.2003.10.257
2. J.W. Yeh, S.K. Chen, S.J. Lin, J.Y. Gan, T.S. Chin, T.T. Shun, C.H. Tsau, S.Y. Chang, Nanostructured high-entropy alloys with multiple principal elements: novel alloy design concepts and outcomes, Advanced Engineering Materials, 6, 5, 2004, 299-303. https://doi.org/10.1002/adem.200300567
3. D. Kumar, Recent advances in tribology of high entropy alloys: A critical review, Progress in Materials Science, 136, 2023, 101106. https://doi.org/10.1016/j.pmatsci.2023.101106
4. X. Liu, J. Zhang, Z. Pei, Machine learning for high-entropy alloys: Progress, challenges and opportunities, Progress in Materials Science, 131, 2023, 101018. https://doi.org/10.1016/j.pmatsci.2022.101018
5. B. Cantor, Multicomponent high-entropy Cantor alloys, Progress in Materials Science. 120, 2021, 100754. https://doi.org/10.1016/j.pmatsci.2020.100754
6. T.R. Somo, M.V. Lototskyy, V.A. Yartys, M.W. Davids, S.N. Nyamsi, Hydrogen storage behaviours of high entropy alloys: a review, Journal of Energy Storage, 73, 2023, 108969. https://doi.org/10.1016/j.est.2023.108969
7. L. Luo, L. Chen, L. Li, S. Liu, Y. Li, C. Li, L. Li, J. Cui, Y. Li, High-entropy alloys for solid hydrogen storage: a review, International Journal of Hydrogen Energy, 50, 2023, 406-430. https://doi.org/10.1016/j.ijhydene.2023.07.146
8. M. Naseri, A.O. Moghadam, M. Anandkumar, S. Sudarsan, E. Bodrov, M. Samodurova, E. Trofimov, Enhancing the mechanical properties of high-entropy alloys through severe plastic deformation: a review, Journal of Alloys and Metallurgical Systems, 5, 2024. 100054. https://doi.org/10.1016/j.jalmes.2024.100054
9. M.J. Sohrabi, H. Mirzadeh, A.R. Geranmayeh, R. Mahmudi, Grain size dependent mechanical properties of CoCrFeMnNi high-entropy alloy investigated by shear punch testing, Journal of Materials Research and Technology, 27, 2023, 1258-1264. https://doi.org/10.1016/j.jmrt.2023.09.313
10. L. Xie, G. Wu, Q. Peng, J. Liu, D. Li, W. Wang, An atomistic study on grain-size and temperature effects on mechanical properties of polycrystal CoCrFeNi high-entropy alloys, Materials Today Communications, 37, 2023, 107264. https://doi.org/10.1016/j.mtcomm.2023.107264
11. G.D. Sathiaraj, C.W. Tsai, J.W. Yeh, M. Jahazi, P.P. Bhattacharjee, The effect of heating rate on microstructure and texture formation during annealing of heavily cold-rolled equiatomic CoCrFeMnNi high entropy alloy, Journal of Alloys and Compounds, 688, 2016, 752-761. https://doi.org/10.1016/j.jallcom.2016.07.155
12. Y. Wu, S. Liu, K. Luo, C. Kong, H. Yu, Deformation mechanism and mechanical properties of a CoCrFeNi high-entropy alloy via room-temperature rolling, cryorolling, and asymmetric cryorolling, Journal of Alloys and Compounds, 960, 2023, 170883. https://doi.org/10.1016/j.jallcom.2023.170883
13. X. Zheng, W. Xie, L. Zeng, H. Wei, X. Zhang, H. Wang, Achieving high strength and ductility in a heterogeneous-grain-structured CrCoNi alloy processed by cryorolling and subsequent short-annealing, Materials Science and Engineering: A, 821, 2021, 141610. https://doi.org/10.1016/j.msea.2021.141610
14. K. Nazaretyan, S. Aydinyan, H. Kirakosyan, D. Moskovskikh, A. Nepapushev, K. Kuskov, M. Tumanyan, A. Zargaryan, R. Traksmaa, S. Kharatyan, AlCo-rich AlCoNiFe and AlCoNiFeCr high entropy alloys: Synthesis and interaction

pathway at high heating rates, Journal of Alloys and Compounds, 931, 2023, 167589. https://doi.org/10.1016/j.jallcom.2022.167589

15. A. Huang, S.J. Fensin, M.A. Meyers, Strain-rate effects and dynamic behavior of high entropy alloys, Journal of Materials Research and Technology, 22, 2023, 307-347. https://doi.org/10.1016/j.jmrt.2022.11.057
16. A. Mohammadi, P. Edalati, M. Arita, J.W. Bae, H.S. Kim, K. Edalati, Microstructure and defect effects on strength and hydrogen embrittlement of high-entropy alloy CrMnFeCoNi processed by high-pressure torsion, Materials Science and Engineering: A, 844, 2022, 143179. https://doi.org/10.1016/j.msea.2022.143179
17. P. Edalati, A. Mohammadi, M. Ketabchi, K. Edalati, Microstructure and microhardness of dual-phase high-entropy alloy by high-pressure torsion: Twins and stacking faults in FCC and dislocations in BCC, Journal of Alloys and Compounds, 894, 2022, 162413. https://doi.org/10.1016/j.jallcom.2021.162413
18. M. Naseri, A. Hassani, M. Tajally, An alternative method for manufacturing Al/B4C/SiC hybrid composite strips by cross accumulative roll bonding (CARB) process, Ceramics International, 41, 2015, 13461-13469. https://doi.org/10.1016/j.ceramint.2015.07.137
19. M. Naseri, M. Reihanian, E. Borhani, Effect of strain path on microstructure, deformation texture and mechanical properties of nano/ultrafine grained AA1050 processed by accumulative roll bonding (ARB), Materials Science and Engineering: A, 673, 2016, 288-298. https://doi.org/10.1016/j.msea.2016.07.031
20. M. Naseri, M. Reihanian, A.O. Moghaddam, D. Gholami, S. Hosseini, M. Alvand, E. Borhani, E. Trofimov, Improving strength-ductility synergy of nano/ultrafine-structured Al/Brass composite by cross accumulative roll bonding process, Journal of Materials Research and Technology, 26, 2023, 6794-6806. https://doi.org/10.1016/j.jmrt.2023.09.046
21. M. Naseri, M. Reihanian, A.O. Moghaddam, D. Gholami, M. Alvand, E. Borhani, E. Trofimov, Insights into the mechanical properties and correlation between strain path and crystallographic texture of the AA2024 alloy during severe plastic deformation, Metals and Materials International, 30, 2023, 412-424. https://doi.org/10.1007/s12540-023-01515-6
22. H. Dong, Y.C. Guo, D. Zhu, G.B. Shan, G.Y. Yang, Y.Z. Chen, In situ observation of destabilization of a nanostructured Ag/Cu multilayer fabricated via multicomponent accumulative roll bonding, Materials & Design, 236, 2023, 112487. https://doi.org/10.1016/j.matdes.2023.112487
23. M.R. Kamali Ardakani, S. Khorsand, S. Amirkhanlou, M. Javad Nayyeri, Application of compocasting and cross accumulative roll bonding processes for manufacturing high-strength, highly uniform and ultra-fine structured Al/SiCp nanocomposite, Materials Science and Engineering: A, 592, 2014, 121-127. https://doi.org/10.1016/j.msea.2013.11.006
24. A. Patel, I. Wani, S.R. Reddy, S. Narayanaswamy, A. Lozinko, R. Saha, S. Guo, P.P. Bhattacharjee, Strain-path controlled microstructure, texture and hardness evolution in cryo-deformed AlCoCrFeNi2.1 eutectic high entropy alloy, Intermetallics, 97, 2018, 12-21. https://doi.org/10.1016/j.intermet.2018.03.007
25. R. Sabban, K. Dash, S. Suwas, B.S. Murty, Strength–ductility synergy in high entropy alloys by tuning the thermo-mechanical process parameters: A comprehensive review, Journal of the Indian Institute of Science, 102, 2022, 91-116. https://doi.org/10.1007/s41745-022-00299-9
26. Y. Wang, J. Chen, R. Ding, W. Wang, J. He, X. Zhou, Effect of cold rolling on microstructure and mechanical property of a novel (Fe50Mn30Co10Cr10)97C2Mo1 high entropy alloy, Journal of Materials Research and Technology, 27, 2023, 6065-6075. https://doi.org/10.1016/j.jmrt.2023.11.064
27. M. Naseri, A.O. Moghaddam, N. Shaburova, D. Gholami, A. Pellenen, E. Trofimov, Ultrafine lamellar microstructures for enhancing strength-ductility synergy in high-entropy alloys via severe cold rolling process, Journal of Alloys and Compounds, 965, 2023, 171385. https://doi.org/10.1016/j.jallcom.2023.171385
28. Y. Ma, L. Sun, Y. Zhang, Z. Zhang, Achieving excellent strength-ductility synergy via cold rolling-annealing in Al-containing refractory high-entropy alloys, International Journal of Refractory Metals and Hard Materials, 114, 2023, 106263. https://doi.org/10.1016/j.ijrmhm.2023.106263
29. L.F. Zeng, R. Gao, Q.F. Fang, X.P. Wang, Z.M. Xie, S. Miao, T. Hao, T. Zhang, High strength and thermal

stability of bulk Cu/Ta nanolamellar multilayers fabricated by cross accumulative roll bonding, Acta Materialia, 110, 2016, 341-351. https://doi.org/10.1016/j.actamat.2016.03.034

30. K. Verstraete, A.L. Helbert, F. Brisset, A. Benoit, P. Paillard, T. Baudin, Microstructure, mechanical properties and texture of an AA6061/AA5754 composite fabricated by cross accumulative roll bonding, Materials Science and Engineering: A, 640, 2015, 235-242. https://doi.org/10.1016/j.msea.2015.05.106
31. W.D. Nix, H. Gao, Indentation size effects in crystalline materials: a law for strain gradient plasticity, Journal of the Mechanics and Physics of Solids, 46, 1998, 411-425. https://doi.org/10.1016/S0022-5096(97)00086-0
32. W. Li, D. Xie, D. Li, Y. Zhang, Y. Gao, P.K. Liaw, Mechanical behavior of high-entropy alloys, Progress in Materials Science, 118, 2021, 100777. https://doi.org/10.1016/j.pmatsci.2021.100777
33. M. Reihanian, M. Naseri, M. Jalili Shahmansouri, Effect of the particle size on the deformation and fracture behavior of Al/4vol.% Al2O3 composite produced by accumulative roll bonding (ARB), Iranian Journal of Materials Forming, 2, 2015, 14-26. https://doi.org/10.22099/IJMF.2015.3237
34. M. Naseri, M. Reihanian, E. Borhani, EBSD characterization of nano/ultrafine structured Al/Brass composite produced by severe plastic deformation, Journal of Ultrafine Grained and Nanostructured Materials, 51, 2018, 123-138. https://doi.org/10.22059/JUFGNSM.2018.02.04
35. A. Fattah-Al Hosseini, M. Naseri, S.O. Gashti, S. Vafaeian, M.K. Keshavarz, A study on passive and electrochemical response of pure nickel in borate buffer solutions: effect of cold deformation, Journal of Materials Engineering and Performance, 27, 2018, 3401-3410. https://doi.org/10.1007/s11665-018-3447-y
36. S. Hashemipour, A. Eivani, H. Jafarian, M. Naseri, N. Park, Microstructure and mechanical properties development of nano/ultrafine grained AISI 316L austenitic stainless steel prepared by repetitive corrugation and straightening by rolling (RCSR), Materials Research Express, 5, 2018, 126519. https://doi.org/10.1088/2053-1591/aae0c1
37. M. Cabibbo, A TEM Kikuchi pattern study of ECAP AA1200 via routes A, C, Bc, Materials characterization, 61, 2010, 613-625. https://doi.org/10.1016/j.matchar.2010.03.007